

# Study on the Gas Retention Capability of Metallic Screens

*Christian Höfflin and Jens Gerstmann*

*German Aerospace Centre, Institute of Space Systems, Bremen*

*Robert-Hooke-Straße 7, 28359 Bremen*

## Abstract

In tank systems of spacecraft's and satellites, metallic screens are found to provide the possibility besides filtering to retain liquid and prevent gas breakthrough by capillary. For determining the maximum retention capability at screens, the so called bubble point, in this study experimental setups are developed to measure the bubble point pressure for metallic screens of type twilled dutch 165 x 1400, 200 x 1400 and 325 x 2300 with isopropyl alcohol, silicon oil and liquid nitrogen. The results are found to follow a linear fit within the investigated regime of fluid properties and are compared with literature values.

## 1. Introduction

The development of advanced cryogenic upper stages for launcher systems like Ariane 5ME leads to new challenges of propellant management in particular for the feature of multiple re-ignitions of the engine and performance during long ballistic flight phases. Due to the cryogen state of the propellants, the tank system has to guarantee the task for gaseous and bubble free supply of the propellants at the requested thermodynamic conditions to the feed system at each time. As cryogen media tend to evaporate very easily even on small heat energy amounts affecting the tank system, the formation of undesired gas phases is very likely. Further, under low gravitational conditions, propellant positioning at the tank outlet for re-ignition becomes a challenge. In this regard, metallic screens have important functions. In addition to the filtering task and the ability to retain liquid in the screen mesh, they are able to hold back gas phases up to a maximum possible gas-to-liquid pressure difference that the screen can withstand, the so called bubble point.

The bubble point is dependent on the screen mesh geometry, its porosity and the fluid properties (gas, liquid) which are additionally dependent on the temperature and pressure conditions. So, the bubble point becomes a characteristic value for screens with regard on the corresponding liquid. Decreasing the porosity leads to an improvement of particle filtration and gas retention but also causes an increase of pressure loss over the screen. For the tank system design, the knowledge of pressure loss and gas retention capability of the used screen is essential to optimize the system for given mission requirements. Therefore the total acceptable pressure loss of the whole tank is not allowed to exceed the bubble point otherwise bubble breakthrough will occur. The importance of the bubble point implies the need for research on the space application relevant screens, which are likely to be used for upcoming tank systems. Although the existing data base on bubble point pressures is wide-ranging in relation to the screen mesh geometries and test liquids, the variation of the literature data does not show a clear behaviour of the bubble point according to its dependencies. Thus, further work has to be done to examine the dependencies between screens and liquids more precisely. For that, an experiment build-up has to be designed, which can provide a reliable measurement technique for the bubble point with regard to the used test liquids and their physical properties and further also allow to measure bubble points under cryogen conditions. New bubble point measurements shall provide an answer on the mentioned dependencies and requirements.

The contribution of this paper focuses on the maximum gas retention capability of metallic screens against gas breakthrough. Experimental studies on twilled dutch screens (165 x 1400, 200 x 1400, 325 x 2300) are presented with isopropyl alcohol, silicon oil and liquid nitrogen. The experimental data for each screen in dependency on the used test liquid will be presented and examined. For each screen a correlation is found and determined between the bubble point and the surface tension  $\sigma$ , which can be described by the function  $\Delta p = f(\sigma)$  in the range from storable to cryogen media.

The following executions will give an overview on state of the art at first. Further, the experiment build-ups will be discussed and defined. The measured results will be presented, compared and discussed with respect to the literature data base.

## 2. State of the Art

The general relation between a gas and a liquid phase forming a capillary surface is given by the Young-Laplace-Equation.

$$\Delta p = \sigma \cdot \left( \frac{1}{r_1} + \frac{1}{r_2} \right) \quad (1)$$

The occurring pressure difference  $\Delta p$  over the gas to liquid interface can be expressed by the surface tension  $\sigma$  and the general radii of curvature  $r_1$  and  $r_2$ . In relation to screens, the Young-Laplace-Equation gains an important relevance for the characterization with regard on the gas retention capability. As screens are fine geometrical structures with pore orifices in micro size dimensions, they are able to use the capillary effect to hold back gas phases in liquid environments. This gas retention capability made screens to be an important component for use in tank systems for space applications. As two-phase flow from tank systems to the engine can result in several undesired problems like cavitation on turbo pumps or propulsion instabilities, screens were implemented to avoid gas phases from leaving the tank systems. Thereby for optimization, design and screen selection purpose, it is essential to find the maximum pressure difference that screens can withstand before bubble breakthrough occurs. This maximum retention capability is defined as the bubble point  $\Delta p_{BP}$  [1].

$$\Delta p_{BP} = \frac{4 \cdot \sigma \cdot \cos(\varphi)}{D_{eff}} \quad (2)$$

The bubble point is dependent on the surface tension  $\sigma$  of the used liquid, the contact angle  $\varphi$ , which is the characteristic parameter for the wettability of a fluid with a solid and gas surface, and the effective pore size diameter  $D_{eff}$ , which approximates the bubble breakthrough surface with an effective circular orifice. Thereby, a special effort has to be focused on the determination of the surface tension  $\sigma$ , as this value is affected by the state variables pressure  $p$  and temperature  $T$ . For accurate estimation of the bubble point the functional dependency of the surface tension  $\sigma = f(p, T)$  has to be known. The influence of the contact angle which is dependent on the liquid, solid and gas combination has to be considered. By the use of fully wetting liquids and suitable cleaning techniques, which are studied by Fester [3], zero contact angles  $\varphi = 0^\circ$  can be achieved. Study relevant test liquids are stated to have zero contact angles for IPA [3], LH<sub>2</sub> [4], LCH<sub>4</sub> [11], LN<sub>2</sub> and LO<sub>2</sub> [12] and SF<sub>0.65</sub> [13]. Gained results of bubble points in combination with these test liquids are achieved with screens made of stainless steel. As the surface tension and the wettability are fluid properties, the effective pore size diameter is defined by the geometrical texture of the screen. This fact implies the need for a detailed investigation on the texture of the twilled dutch woven screens to understand the relation between the real breakthrough orifice and the effective pore size diameter.

Over the past decades of space mission studies and applications screens were established as method for expulsion and acquisition of propellants from tank systems. In the 1970s, an orbital manoeuvring system (OMS) as well as the reaction control system and the auxiliary power unit of the space shuttle (SS/RCS and SS/APU) were studied by Fester [2], [3]. On the parametric evaluation of screen devices using square and twilled dutch screens for OMS the dependency of the design on mission relevant factors like flexibility, performance and system mass were identified. Further, the evaluation of propellant properties and their bubble point pressures used in the RCS and APU resulted in more detailed information on screen performance being also dependent on screen contamination, cleaning technique and propellant properties like contact angle. Simultaneous to Festers work, Cady [4], [5], [6] studied a thermodynamic vent system (TVS) and a wall screen liner (WSL) for orbital storage and transfer of liquid hydrogen. The experimental and analytic investigations included the survey of several screens similar to Fester's screen selection for their performance parameters like the bubble point pressure and the heat flux influence which were found to be important factors for the tank system design. Six tank system designs were weight optimized. As the main weight is contributed by the chosen screen device, the optimization required the lightest screen with the best performance characteristics for the chosen mission duration. Further Cady [7] provides a study on an analytical design tool, which is verified by experimental data like bubble point measurements, to predict transient effects like pressure surge on the gas retention performance of screen systems.

In the present, space mission applications undergo an increasing demand for the usage of cryogen propellants. This requirement establishes the focus on detailed and expanded investigations on all corresponding techniques which are needed to enable, implement and optimize tank systems for cryogen propellant storage and propellant delivery to the engine in low gravity environments. Based on the work of Fester and Cady and the on-going Space Shuttle program

until 2012, the demand for cost and risk reduction forced the replacement of the previously used toxic propellants by non-toxic. Due to the alternative propellant combination of ethanol and liquid oxygen, the interest in cryogen propellant application has been forced and a program was established to evaluate screen performance characteristics. First results are presented by Chato & Kudlac [8]. An experiment build-up for the measurement of twilled dutch screens is developed to achieve and extend the screen bubble point data base with isopropyl alcohol (IPA), liquid nitrogen (LN<sub>2</sub>) and liquid hydrogen (LH<sub>2</sub>). As this work does only present liquid nitrogen data as a simulant for liquid oxygen, the experiment build-up was redesigned for measurements with liquid oxygen (LO<sub>2</sub>). The results for LO<sub>2</sub> with additional data on IPA and LN<sub>2</sub> are presented by Kudlac & Jurns [9]. On the course of space application developments, NASA further determined liquid methane (LCH<sub>4</sub>) to be a promising option for future exploration missions. The question for a new cryogen propellant being usable for space applications led to the experimental investigation of screen characteristics with LCH<sub>4</sub>. By a further redesign of the experiment build-up, Jurns, McQuillen, Gaby and Sinacore [10], [11] were able to measure screen bubble points with LCH<sub>4</sub> under normal boiling pressure and sub-cooled conditions. The condition of a sub-cooled cryogen state forced Jurns & McQuillen [12] to extend their investigations to LO<sub>2</sub> in a sub-cooled, normal boiling point and warm fluid condition with additional IPA measurements to examine this states and their influence on the bubble point.

The latest work on bubble point investigations are done by Conrath [13]. The study is focused on the effect of dynamic fluid conditions on the bubble point. The results show an influence of the measurement conditions on the accurate prediction of the gas bubble breakthrough based on experimental investigations with varying mass flows. Therewith, Conrath was able to determine a criterion for bubble growth dependent on the bubble forming mass flow.

Overall, the evaluation of the literature show results on bubble point pressures for twilled dutch 200 x 1400 and 325 x 2300 screens which are summarized and plotted in Fig. 1. The presented data base spreads and varies over a wide range of studied liquids.

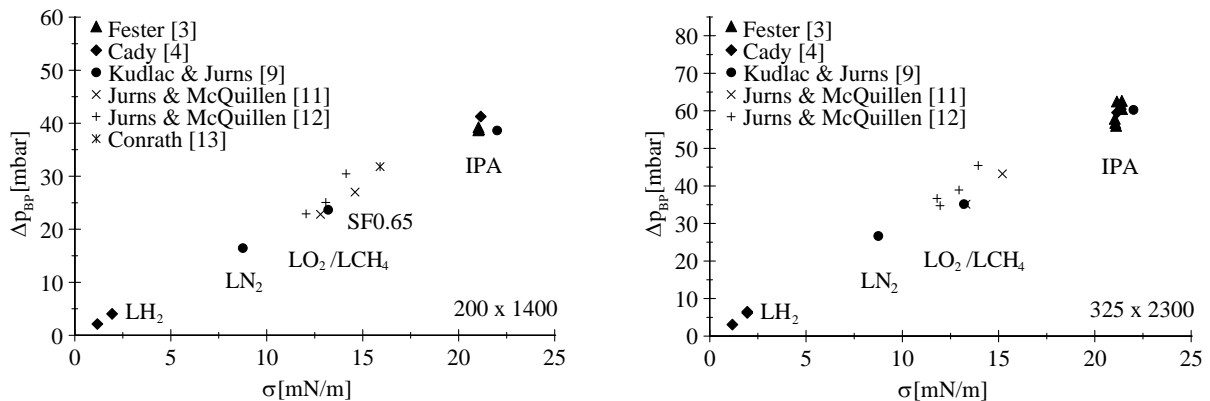


Figure 1: Literature bubble point data for twilled dutch screens 200 x 1400 and 325 x 2300

The variations can be addressed to several reasons in general. First, as gas bubble breakthrough occurs at the weakest orifice of the screen, the location of the breakthrough can be located anywhere on the tested screen sample. Therefore, an experiment build-up with screens being measured in a vertical and fully dipped condition is inapplicable, as the unknown breakthrough location is affected by a hydrostatic head pressure and so a precise estimation of the hydrostatic head and therewith the bubble point can be very difficult and lead to inconsistent results. Further, an experiment build-up which measures screen bubble points against the buoyancy direction of gas bubbles can lead to a trapped bubble under the screen, so a continuous bubble breakthrough measurement is not possible. With regard on the screen mesh geometry, the weakest orifice can vary within the manufacturing accuracy, as the generation of screen meshes underlie an inaccuracy so the weakest screen orifice can vary in dimension. A special look has to be taken at the attachment for screen samples to the experiment setup. As the screen textures are of micro size dimension, the attachment and sealing of screens, which are normally obtained by contact forces, can lead to an undesired mechanical deformation of the screen and hence to a change in the screen orifice. This effect will be discussed in Chapter 3.5 within the presented work. Beside measurement and production influences, Fester [3] identified the effect on screen cleanliness to be very essential for accurate measurements as pollutions can influence the orifice geometries and wettability of liquids on the screen surfaces. Also the choice of cleaning materials and the cleaning process, which shall be done to remove contaminants, can result in an incorrect measurement due to the effect, that cleaning materials can result in a converse effect of screen pollution instead of

cleaning. Further, an incorrect determined surface tension  $\sigma$  can generate inconsistent bubble point data. As the surface tension is dependent on the temperature and pressure state during the experiment, the determination of pressure and temperature conditions is very important.

Due to the wide scatter of the data base and the possible reasons for an inaccurate measurement of the bubble point new precise experimental investigations on space application relevant twilled dutch screens are done with isopropyl alcohol (IPA), silicon oil (SF0.65) and liquid nitrogen ( $\text{LN}_2$ ) to examine the influence of surface tension variation on the bubble point and if results are scalable within the studied surface tension region. The following executions will give an overview on the experiment set up at first. Further, the screen texture and screen preparation for the measurement are discussed and described followed by the measurement conditions and fluid property estimations. To qualify the accuracy of the experiment setup a validation is presented. Achieved results are analysed, evaluated and compared to the literature to give an answer about the quality of the measurements to existing data.

### 3. Experiment setup

The experiment setup is separated into two different parts for the measurement with room temperature storable liquids like IPA and SF0.65 and the measurement with the cryogen  $\text{LN}_2$ . The setup is discussed in the following sections.

#### 3.1 Setup for test liquids IPA and SF0.65

For the bubble point measurements with IPA and SF0.65 the experiment build-up is shown in Fig. 2. The experiment consists of a test chamber, which is separated by the screen into two regions where the lower part will form a complete closed volume by the chamber and the screen and the upper part, which is open to ambient conditions. For temperature measurement and He supply a temperature sensor T and a gas supply tube, connected to the mass flow actuator F, is led through the chamber wall into the closed volume region. For the pressure measurement a differential pressure transducer D is connected to the gas supply tube on the one side and to ambient conditions on the other. The ambient pressure  $p_0$  is controlled by the absolute pressure transducer A.

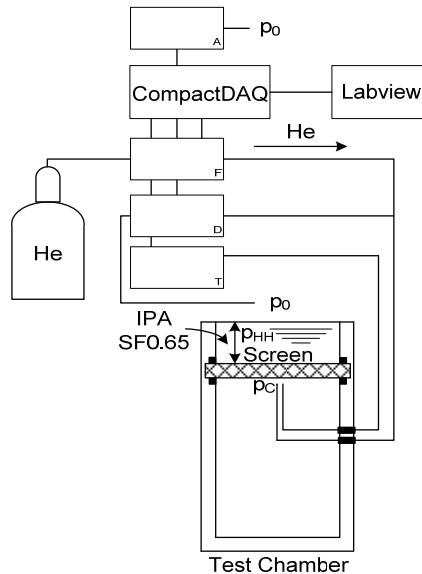


Figure 2: Experimental setup for IPA and SF0.65

For the measurement, the chamber volume is rinsed by helium to remove undesired gas phases and to guarantee the pressurization of the chamber. Then, the upper part of the chamber is filled with IPA or SF0.65 to the edge of the chamber top with a fill height of 12mm. This leads to the effect of a constant hydrostatic head  $p_{HH}$ , which can be calculated over the known distance of the screen to the chamber top and the corresponding fluid density at the present absolute pressure  $p_0$  and temperature condition. As IPA and SF0.65 are volatile liquids, the hydrostatic head has to be kept constant by a continuous supply of liquid. By the continuous mass flow of helium into the closed chamber volume, the chamber pressure  $p_C$  starts to increase, trying to push the gas phase through the screen into the

liquid. Due to the bubble point, the pressure has to be increased to a maximum value  $p_{CM_{max}}$ , where bubble breakthrough occurs. At breakthrough, the chamber pressure starts to drop, as helium gas bubbles are released into the liquid. Finally, the bubble point pressure  $\Delta p_{BP}$  can be achieved by solving of the following equation.

$$p_{CM_{max}} = \Delta p_{BP} + \Delta p_{FL} + \Delta p_{HH} + p_0 \quad (3)$$

The factor  $\Delta p_{FL}$  is contributed by the friction loss of helium gas flow through the supply tube. This factor will be discussed in the results and shown to be negligible. As the difference  $p_{CM_{max}} - p_0$  is the measured signal of the differential pressure transducer D, the bubble point results in the correction of the measured signal by the constant hydrostatic head pressure  $\Delta p_{HH}$ .

### 3.2 Setup for cryogenic test liquid LN<sub>2</sub>

For the bubble point measurements with LN<sub>2</sub> the experiment build-up is shown in Fig. 3. For the measurement under constant LN<sub>2</sub> temperature conditions, the test chamber is attached to a Dewar and insulated to minimize temperature influence. After the chamber volume is rinsed by helium to remove undesired gas phases, the Dewar is filled with LN<sub>2</sub> until the test chamber is fully immersed. To compensate evaporation and a possible uncovering of the test chamber, the fill level has to be adequate. This leads to the problem of an unstable hydrostatic head pressure  $\Delta p_{HH}$  above the screen. For solving of equation (3), the hydrostatic head has to be known for each bubble breakthrough measurement.

To determine the hydrostatic head  $p_{HH}$ , a temperature sensor T is attached to a distance measurement device and adjusted so that the zero level matches with the screen surface. As the Dewar is filled with LN<sub>2</sub>, the liquid surface can be detected with the temperature sensor and so the distance between the screen and the liquid surface. As the absolute pressure transducer A detects the ambient pressure  $p_0$ , the density for saturated LN<sub>2</sub> conditions can be determined by REFPROP [15].

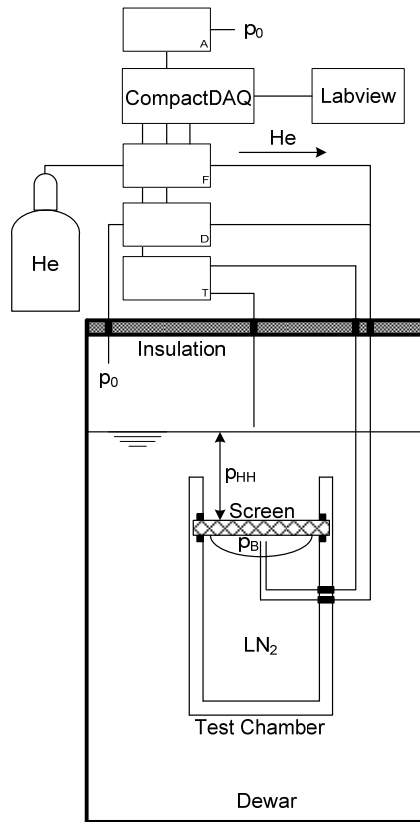


Figure 3: Experimental setup for LN<sub>2</sub>

By continuous helium gas flow into the test chamber a helium gas bubble is formed under the screen, which displaces LN<sub>2</sub> until the whole screen is covered by the gas bubble and the bubble pressure  $p_B$  starts to increase until the maximum pressure  $p_{BMax}$  is reached where bubble breakthrough occurs. Finally the bubble point can be calculated by solving of equation (3).

### 3.3 Instrumentation and system error

The instrumentation for both build-ups consists of the same components, whereby the LN<sub>2</sub> build-up is extended with a temperature sensor T for the measurement of the hydrostatic fill level above the screen. The instrumentation consists of the absolute pressure transducer A, the mass flow actuator F, the differential pressure transducer D and the temperature sensors T. For data acquisition and storage by Labview, the analogue component and control signals are converted by NI CompactDaq analog/digital modules. To give an answer about the quality of the measurement signals, the accuracy of each component has to be taken in account to determine the component errors  $\Delta p_{COMerr}$  on the signal transmission path. The components are listed in Tab. 1.

Beside the systematic errors of the system components, also possible random errors have to be identified. Because pressure and temperature conditions are normally inconsistent over the experiment duration, a variation of the liquid properties has to be taken in account. To derive the variation of surface tension caused by changing temperatures and pressures during measurement, the average deviation of the mean temperature is used to estimate surface tension variation by REFPROP [15]. The surface tension variation leads to a defective estimation of the bubble point pressure  $\Delta p_{BPerr}$ . Further, random errors can also be caused by the operator himself, when measuring hydrostatic heads on the LN<sub>2</sub> and IPA/SF0.65 experiments. To estimate the error on the hydrostatic head pressure  $\Delta p_{HHerr}$ , the maximum deviation on each measurement was identified to be 1mm for IPA/SF0.65 and 1.5mm for LN<sub>2</sub> measurements.

Table 1: Experiment component data

	Component Type	Measurement Range	Accuracy
Absolute Pressure Transducer A	MKS Baratron Type 627B	0 – 1.33bar	± 0.12% of reading value
Mass flow actuator F	MKS 1179B Analog	0 – 1.77SCCM He	± 0.5% of measuring value + 0.2% of final value
Differential Pressure Transducer D	MKS Baratron Type 120	0.1 – 30000mbar	± 0,12% of measuring value (standard)
Temperature Sensors T	Thermocouple Thermocoax FKI 05/50	-200°C – 1000°C	± 1.5°C up to 375°C ± 0.75°C from 375°C to 1000°C
CompactDaq Pressure & Mass Flow Module	NI 9239	Voltage: -10V – 10V	19mV
CompactDaq Temperature Module	NI 9211	Voltage: -80mV – 80mV	< 0.07°C on measured value

The average error  $\Delta p_{err}$  on each bubble point measurement is given by the arithmetic mean of the summary of the hydrostatic head pressure  $\Delta p_{HHerr}$ , bubble point pressure  $\Delta p_{BPerr}$ , friction loss  $\Delta p_{FLerr}$  and the sum of component errors  $\Delta p_{COMerr}$ .

$$\Delta p_{err} = \Delta p_{HHerr} + \Delta p_{BPerr} + \Delta p_{FLerr} + \Sigma \Delta p_{COMerr} \quad (4)$$

As discussed in the results, the friction loss error  $\Delta p_{FLerr}$  will be shown to be negligible.

### 3.4 Twilled dutch screen texture

Due to the importance of the geometrical texture of screens on the bubble point, the geometry of the twilled dutch woven screen will be presented in detail. The geometrical texture is shown in Fig. 4.

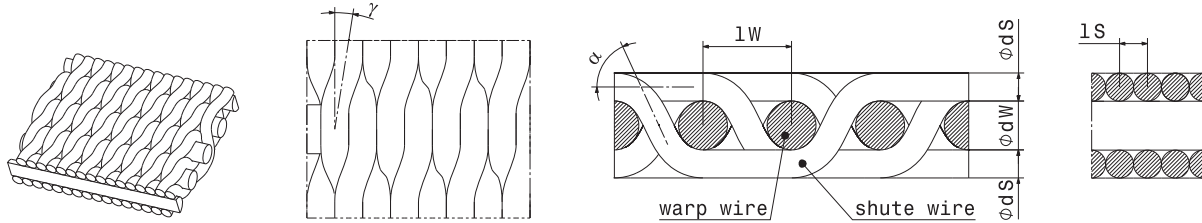


Figure 4: Geometry of a twilled dutch screen

The geometry of the twilled dutch screen is defined by the numbers of wires per inch, the diameters  $dS$ ,  $dW$  of the warp and shute wires and the specific twilled dutch weave. Thereby a shute wire passes two warp wires before the pathway changes to run under them for two warp wires and then coming back up. This behaviour is steadily. Further, the shute wires underlie an alternating shift along their thread path. Therewith, geometrical connections like the warp and shute wire distance  $1W$ ,  $1S$ , the shute wire bend angle  $\alpha$  and the shute wire shift angle  $\gamma$  can be determined. An additional factor for the screen definition is the so called grade of filtration. This value describes the maximum spherical particle size, which can pass through a screen. With regard on the definition of the effective pore size diameter  $D_{eff}$ , it seems to be obvious, that the grade of filtration corresponds with the effective diameter and therefore determines the orifice diameter of the bubble breakthrough. However, according to investigations of Cady [4] and Jurns & McQuillen [12] they do not seem to correlate with each other.

Further, the knowledge of the determinable screen data implies the possibility of a mathematical estimation of the grade of filtration, which is normally measured with the glass bed test, and the effective diameter, which is determined by bubble point measurements. In the case of twilled dutch, it has to be mentioned, that the shute wires undergo a mechanical deformation because the numbers of shute wires for twilled dutch lying within one inch is too large to pack them parallel in a non-deformed condition. Therefore a mathematical estimation will become a challenge. The study relevant twilled dutch screen data are given in Tab. 2.

Table 2: Twilled dutch screen data

	Warp wires	Shute wires	Diameter Warp Wire [ $\mu\text{m}$ ]	Diameter Shute Wire [ $\mu\text{m}$ ]	Grade of filtration [ $\mu\text{m}$ ]	
	165 x 1400 <sup>ab</sup>	165	1400	70	40	21
	200 x 1400 <sup>ab</sup>	200	1400	70	40	14
	325 x 2300 <sup>ab</sup>	325	2300	38	25	10

<sup>a</sup> Stainless steel <sup>b</sup> Screen data provided by Spörl KG

Due to the presented facts, the bubble point and effective pore size diameters will still have to be estimated experimentally.

### 3.5 Screen sample preparation

The screen sample preparation is essential for the accurate measurement of the bubble point. The sample consists of a 42mm diameter disc and is attached to the test chamber by a screen seat. To ensure that the gas phase has to pass the screen, the disc is sealed at the edges with indium. However, first measurements yielded to bubble breakthrough near the indium seal with lower bubble points than expected. This effect was probably caused by screen deformation according to the indium seal. Due to the subtlety of the screen geometry and the fact, that the indium has to be deformed to achieve adequate sealing, it was assumed that deformation forces caused an undesired screen deformation. To avoid this effect, the screen disc is stabilized by soldering of the edges where the indium seals are located and to ensure that bubble breakthrough occurs in the centre of the screen sample. For accurate measurement of bubble point pressures, the screen sample preparation is very important to avoid deformations and thus incorrect

measurements. Further each screen sample is cleaned by a 10 minute ultrasonic bath at 60°C in one litre deionised waters with 10g Turco 4215 NC (10g/l). Afterwards the samples are rinsed with IPA and attached to the screen seat.

### 3.6 Measurement mass flow and friction loss

The generation of the bubble breakthrough is directly influenced by the mass flow, which pressurizes the screens in the experiments. For an adequate bubble point measurement, the mass flow value is essential to generate an optimum bubble growth and single bubble detach from the weakest screen orifice at the screen surface. Further, the mass flow influences the generated friction loss in the supply tube.

As the mass flow is not allowed to be too high with respect on the friction loss and also not too low with respect on an accurate measurement and measurement duration, the mass flow has to be chosen properly with respect on these requirements. To measure adequately, a gas bubble has to reach a specific volume where buoyancy forces are in balance with surface tension forces to be able to detach into the liquid. For the detachment of a gas bubble from a single orifice, the bubble growth has to be slow, so detaching is dominated by buoyancy. In this regard, Conrath [13] studied the influence of the mass flow on the bubble detach and bubble point pressure measurement for twilled dutch 200 x 1400. His result presents a mass flow of  $1\text{mm}^3/\text{s}$  to be applicable for adequate bubble point measurements, which is accepted to be valid for measurements within this work. The mass flow for every bubble point measurement was thereby set to 0.05SCCM which lies below  $1\text{mm}^3/\text{s}$ .

The friction loss  $\Delta p_{FL}$  which is generated by the chosen mass flow  $\dot{V}$  can be calculated by equation (5) for steady laminar flow through tubes with circular cross section [14]. As the tube geometry is given by its length  $l_R$  and radius  $r_R$ , the viscosity  $\eta_{He}$  of the pressurant (Helium) can be calculated at the experiment pressure  $p$  and temperature  $T$  conditions with REFPROP [15]. The maximum friction loss is thereby generated under ambient conditions. Thus, the friction loss lies below 0.085mbar for all measurements.

$$\Delta p_{FL} = \frac{8 \cdot \dot{V} \cdot \eta_{He} \cdot l_R}{\pi \cdot r_R^4} \quad (5)$$

Compared to the lowest bubble point value, the maximum percentage of the friction loss on the measured bubble points is equivalent to 0.35% or below. Thereby, the friction loss and its influence on the measurement error  $\Delta p_{FLerr}$  are considered to be negligible for all measurement results.

### 3.7 Data compilation and fluid properties

For an accurate comparison and evaluation of measurement and literature data, the dependency of the surface tension  $\sigma = f(p, T)$  is very important. As temperature and pressure conditions are determined during test sequence, the surface tension can be determined for LN2 by REFPROP [15], IPA by VDI-Wärmeatlas [16] and SF0.65 by Landolt & Börnstein [17]. Thereby, the surface tensions for IPA and SF0.65 are presented to be only a function of the temperature  $T$   $\sigma_{IPA/SF0.65} = f(T)$  and are determined by linear extrapolation between given data points.

For comparison purpose, only literature data was used, which either provides temperature and pressure conditions to allow surface tension calculations or direct surface tension data which was determined or presented for the corresponding bubble point value. These restrictions qualified the comparison of the literature data from Fester [3] for IPA, Cady [4] for IPA and LH<sub>2</sub>, Kudlac & Jurns [9] for IPA, LN<sub>2</sub> and LO<sub>2</sub>, Jurns & McQuillen [11], [12] for LO<sub>2</sub> and LCH<sub>4</sub> and Conrath [13] for SF0.65.

### 3.8 Validation

To give an answer on the functionality of the experiment build-ups, stainless steel discs with a 42mm diameter and a single orifice in the disc centre, which are shown in Fig. 5, are created by a laser optic procedure. The geometry of the circular orifices is examined by a scanning electron microscope. The two main axis diameters of the orifices are measured and given by  $L1/L2$ . For these orifices the bubble point pressures were measured with IPA. According to Young-Laplace and the property of IPA to be a fully wetting liquid, the two main axis diameters are assumed to correlate with the curvature of radii of the forming gas bubble at maximum pressure before bubble breakthrough occurs. Therefore the bubble point pressure of the orifices can be calculated by equation (1) with the surface tension

of IPA extrapolated from data given by VDI-Wärmeatlas [16] at the corresponding temperature condition of IPA at ambient pressure. The dependency of the radii of curvature from the main axis diameters are given by  $r_1 = L1/2$  and  $r_2 = L2/2$ .

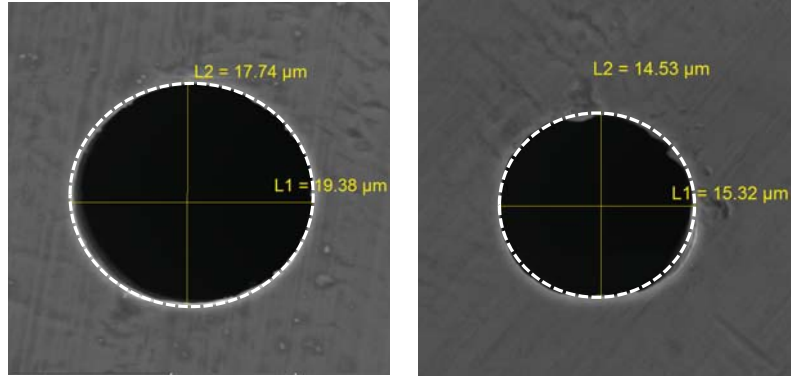


Figure 5: Microscope photos of investigated test pores of different diameter with two main radii.  
The white dashed line corresponds to the pore edge

The results presented in Tab. 3 show that the theoretical bubble points are in good agreement to the measured bubble point with the IPA/SF0.65 experiment build-up. The deviation of the measured to the calculated values lies below 2.43% and 0.33% for the circular orifices.

Table 3: Calculated and measured bubble point for elliptic and circular orifice

		Av. Temperature [°C]	Surface Tension IPA [mN/m]	$r_1$ [μm]	$r_2$ [μm]	Bubble Point [mbar]
Circular	Measured	22				47.01 <sup>a</sup>
	Calculated	-	21.24	9.69	8.87	45.87
Circular	Measured	23				56.94 <sup>b</sup>
	Calculated	-	21.16	7.66	7.265	56.75

<sup>a</sup> Average error  $\Delta p_{err} = 0.33\text{mbar}$ , <sup>b</sup> Average error  $\Delta p_{err} = 0.39\text{mbar}$

## 4. Results

The results of the bubble point measurements of the twilled dutch screens 165 x 1400, 200 x 1400 and 325 x 2300 with IPA, SF0.65 and LN<sub>2</sub> are presented and discussed hereinafter. The contribution and influence of measurement parameters are identified and taken in account on the accurate determination of bubble point values. The data evaluation will be described, discussed and compared to usable literature values.

### 4.1 Data evaluation and discussion

Table 4: Measurement results with standard deviation and average measurement error

		165 x 1400		200 x 1400		325 x 2300
IPA	$\Delta p_{BP}$ [mbar]	35.75		48.55		68.81
	$\Delta std$ [mbar]	0.56		0.23		0.37
	$\Delta p_{err}$ [mbar]	0.21		0.47		0.45
SF0.65	$\Delta p_{BP}$ [mbar]	25.93		35.84		50.62
	$\Delta std$ [mbar]	0.44		0.16		0.07
	$\Delta p_{err}$ [mbar]	0.25		0.26		0.32
LN2	$\Delta p_{BP}$ [mbar]	15.09	14.98	19.58	20.02	29.27
	$\Delta std$ [mbar]	0.04	0.06	0.10	0.05	0.10
	$\Delta p_{err}$ [mbar]	0.32	0.35	0.53	0.53	0.58

For the validity of the achieved results each measurement consists of an arithmetic mean of 9 single bubble point measurements with a calculated standard deviation  $\Delta std$ . Each error  $\Delta p_{err}$  is calculated as arithmetic mean, which is discussed in Chapter 3.3. The deviation on the error calculation was below 1 Pascal and thus neglected for the estimation of the total error. In conclusion the accuracy of the measurements is given by the sum of the standard deviations and the measurement errors. The results of the bubble point measurements with their standard deviations  $\Delta std$  and measurement errors  $\Delta p_{err}$  are presented in Tab. 4.

The surface tension values  $\sigma$  are calculated for the arithmetic mean of the measured temperature  $T$  and pressure  $p$  as described in Chapter 3.7. The surface tension values and the pressure and temperature conditions are presented in Tab. 5. For the evaluation and comparison to literature values, the results are plotted in a surface tension-bubble point-diagram for 165 x 1400, Fig. 6, 200 x 1400, Fig. 7 and 325 x 2300, Fig. 8. For each screen, a fit is found which approximates the bubble point values in dependency of the surface tension within the determined tolerances. The fits follow a linear behaviour with the slope of the fit line  $m$  according to the function  $\Delta p_{BP} = m \cdot \sigma$ . Compared to equation (2) the variable  $m$  describes the correlation with the effective pore size diameter  $D_{eff}$  as  $m = 4/D_{eff}$  for the used test liquids. The slopes of the fit line and the corresponding effective pore size diameters are presented in Tab. 6.

Table 5: Surface tension data at pressure and temperature conditions

		<b>165 x 1400</b>	<b>200 x 1400</b>	<b>325 x 2300</b>		
IPA	$p$ [mbar]	993.75	994.14	990.63		
	$T$ [K]	294.59	295.23	294.81		
	$\sigma$ [mN/m]	21.25	21.20	21.23		
SF0.65	$p$ [mbar]	989.32	978.27	980.80		
	$T$ [K]	295.21	294.70	294.51		
	$\sigma$ [mN/m]	15.77	15.81	15.82		
LN2	$p$ [mbar]	992.18	991.87	1001.03	990.86	995.98
	$T$ [K]	76.64	76.76	76.58	76.85	76.86
	$\sigma$ [mN/m]	8.92	8.92	8.88	8.89	8.88

This correlation between the effective pore size diameter and the slope of the fit line shows, that the bubble formation is equal for the used test liquids IPA, SF0.65 and LN<sub>2</sub> at the corresponding screen and proofs, that the scalability of the bubble point values within the studied test liquids is possible and valid according to equation (6).

$$\left. \frac{\Delta p_{BP}}{\sigma} \right|_{Screen} = const. \quad (6)$$

Table 6: Slopes of the fit line  $m$  and the effective pore size diameter  $D_{eff}$ 

	<b>165 x 1400</b>	<b>200 x 1400</b>	<b>325 x 2300</b>
$m$ [ $10^5/m$ ]	1.67	2.26	3.22
$D_{eff}$ [ $\mu m$ ]	23.95	17.70	12.42

Further, the effective pore size diameter is compared with the grade of filtration, presented in Tab. 2. The values do not correlate with each other as predicted by Cady and Jurns & McQuillen, mentioned in Chapter 2, and show, that the gas breakthrough orifice is either of larger circular size or elliptic with one of the main axis diameters being larger than the grad of filtration diameter. Using the grade of filtration for bubble point prediction will lead to an overestimation of the value.

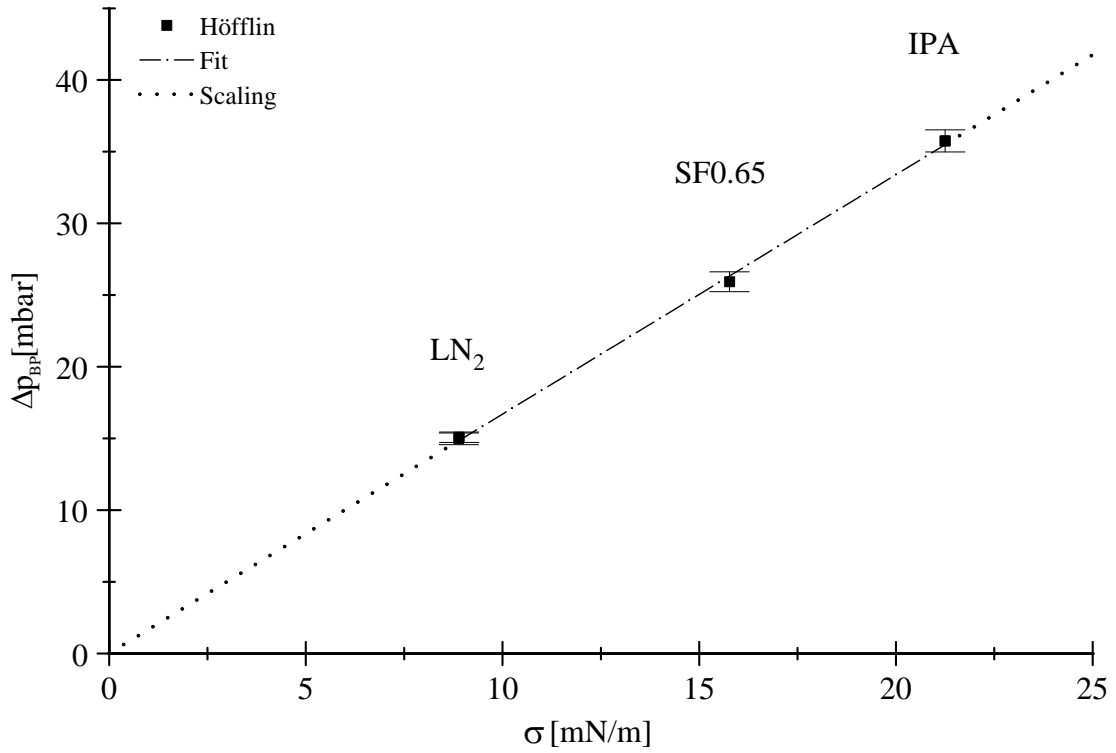


Figure 6: Measured bubble point in dependence on the surface tension for the screen 165 x 1400

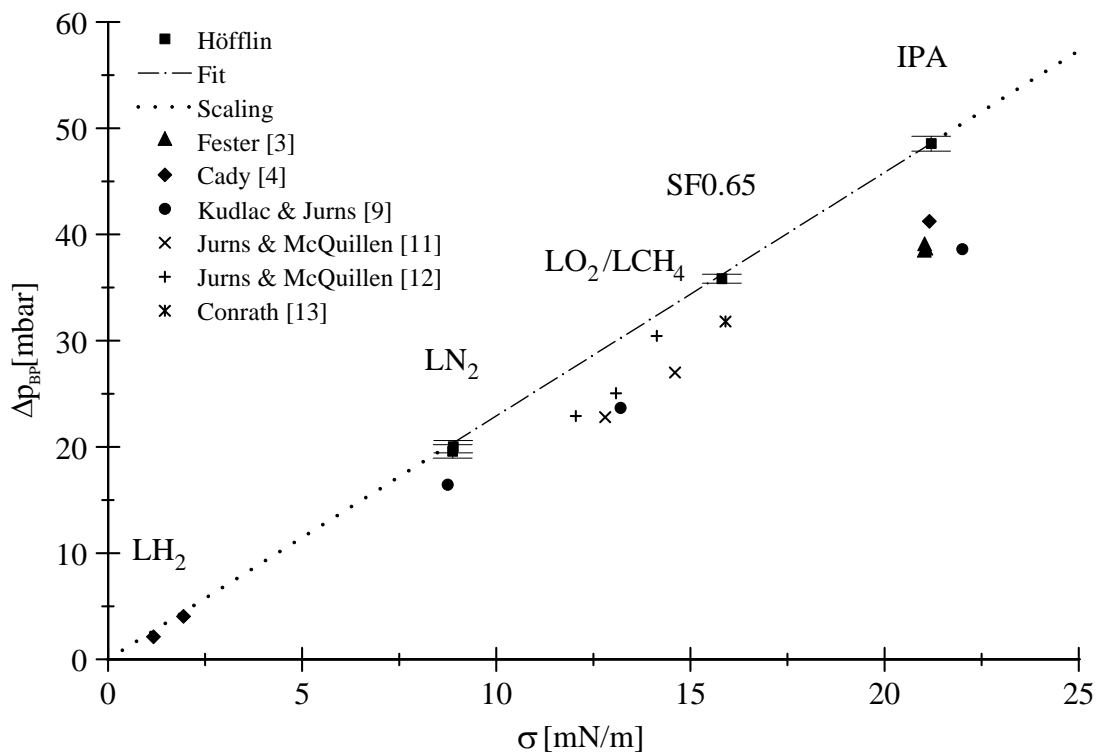


Figure 7: Measured bubble point in dependence on the surface tension for the screen 200 x 1400

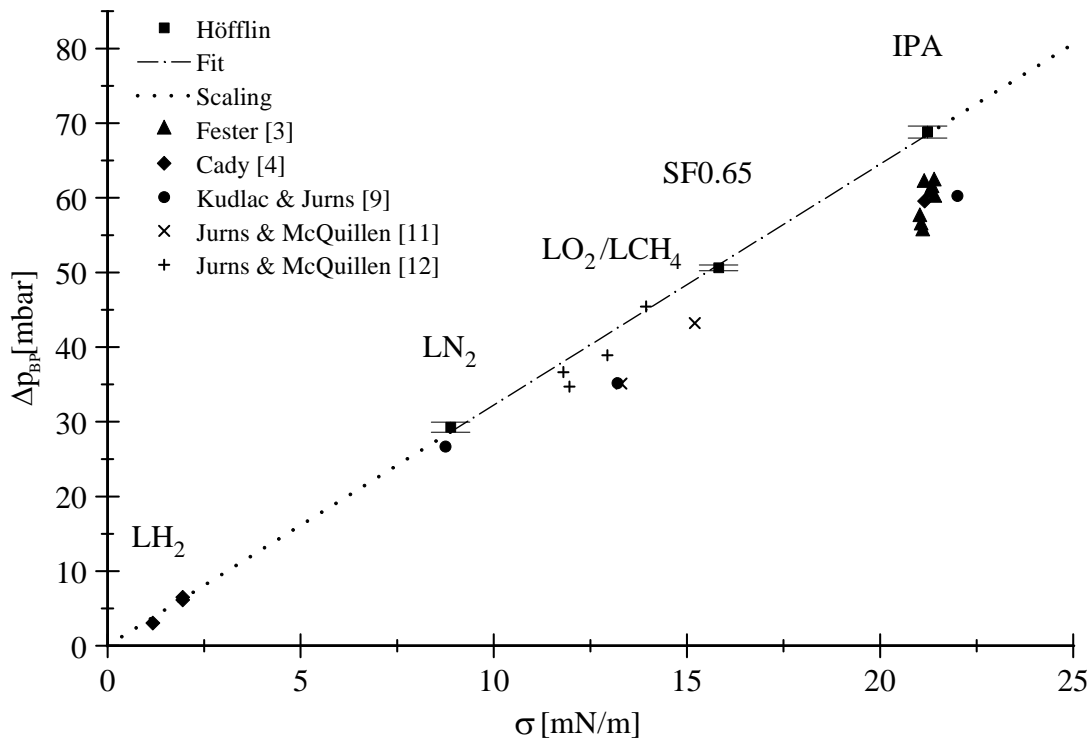


Figure 8: Measured bubble point in dependence on the surface tension for the screen 325 x 2300

Beside the mentioned results, it can be seen, that there is no existing literature data for the twilled dutch 165 x 1400 screen. The presented results in Tab. 5 and Fig. 6 are the first available bubble point data for this screen.

Further, the literature values for twilled dutch 200 x 1400 and 325 x 2300, presented in Fig. 1, are integrated to the results shown in Fig. 7 and Fig. 8. Good correlations are found for  $\text{LH}_2$  data for both 200 x 1400 / 325 x 2300 and  $\text{LN}_2$  and  $\text{LO}_2$  data for 325 x 2300. But, bubble point data for  $\text{LN}_2$ ,  $\text{LCH}_4$ , SF0.65 and IPA are also found to be well below the achieved measurement results and fit curves. The reasons for this deviations and variations of the literature values to the experiment results may refer to the discussion within Chapter 2.

Beside the results achieved in this work, the performance of screens during mission execution has to be taken in account to finally qualify the usability of screens for the application in upper stages. As tank systems are affected by vibrations during mission execution and screens are permanently stressed by forces due to continuous outflow of propellant from the tank system, which can lead to a slow progressive deformation of the screen geometry, degradations of the screen mesh and the performance characteristics are likely to occur. To compensate degradation effects, tank systems are designed with safety factors to guarantee that their total acceptable pressure loss is not allowed to overcome the bubble point during mission execution at any time.

## 5. Summary

This paper presents experimental results on the bubble point pressure for twilled dutch screens 165 x 1400, 200 x 1400 and 325 x 2300 with isopropyl alcohol, silicon oil and liquid nitrogen. Further, the experimental setup is described with all corresponding measurement components and their accuracy. The test sequence and measuring track are identified and explained to be solved for bubble point estimation as well as the overall error which is given by the summary of random and systematic errors and calculated for every measurement. The texture of the twilled dutch screens is defined in detail and all relevant screen data is presented. In regard on the screen texture, the screen sample preparation is described to identify and show possible problems for measurement. A special focus was thereby set on the mass flow for adequate bubble detachment and pressure measurement and the determination of the surface tension as this parameter is dependent on temperature and pressure conditions and thus very important to be determined accurately. Further, to show the accuracy of the whole experiment setup, a validation is presented with circular single orifice screens which present measured bubble point values as theoretical calculated. The measurement and surface tension results are summarized and plotted for evaluation and discussion. The measured

bubble point values are found to follow a linear fit curve within the estimated tolerances for each screen and are scalable with each other within the used test liquids and the corresponding screen. As the slope of fit line is equivalent to the inverse of the effective pore size diameter, the effective pore size diameters are compared to the grades of filtration and found to not correlate with each other. This result agrees with literature statements. The comparison of the measurement results to literature values shows a good agreement to LN<sub>2</sub>, LH<sub>2</sub> and LO<sub>2</sub> data for 200 x 1400 and 325 x 2300 twilled dutch. But data for LN<sub>2</sub>, LCH<sub>4</sub>, SF<sub>0.65</sub> and IPA are also shown to be well below the achieved measurement results and the linear fit curves. Reasons for the data deviation and variation are identified and discussed. As there is no comparable literature data for the 165 x 1400 twilled dutch, the presented bubble point results for IPA, SF<sub>0.65</sub> and LN<sub>2</sub> are the first available data for this screen type.

## References

- [1] Frank T. Dodge. The new “dynamic behaviour of liquids in moving containers”. Southwest Research Institute. San Antonio. Texas. 2000.
- [2] D. A. Fester., et al. Acquisition/Expulsion System for Earth Orbital Propulsion System Study. Final Report. Volume V - Earth Storable Design. MCR-73-97 (Vol. V). Martin Marietta Corporation. Denver. Colorado.
- [3] D. A. Fester., et al. SS/RCS Surface Tension Propellant Acquisition/Expulsion Tankage Technology Program. Interim Report. NASA CR-140299. August 1974.
- [4] E.C. Cady. Study of thermodynamic vent and screen baffle integration for orbital storage and transfer of liquid hydrogen. NASA CR-134482. Final Report. August 1973.
- [5] E.C. Cady. Design and evaluation of thermodynamic vent/screen baffle cryogenic storage system. NASA CR-134810. Final Report. June 1975.
- [6] E.C. Cady. Design of thermodynamic vent/screen baffle cryogenic storage system. J. Spacecraft. Vol. 12. No. 8. August 1975.
- [7] E.C. Cady. Effect of transient liquid flow on retention characteristics of screen acquisition system. NASA CR-135218. Final Report. April 1977.
- [8] David J. Chato., and Maureen T. Kudlac. Screen Channel Liquid Acquisition Devices for Cryogenic Propellants. AIAA-2002-3983. June 2005.
- [9] Maureen T. Kudlac., and John M. Jurns. Screen Channel Liquid Acquisition Devices for Liquid Oxygen. AIAA 2006-5054.
- [10] John M. Jurns., John B. McQuillen., Joseph D. Gaby Jr., and Steven A. Sinacore Jr.. Bubble Point Measurements With Liquid Methane of a Screen Channel Capillary Liquid Acquisition Device. NASA/TM-2009-215494.
- [11] John M. Jurns., and John B. McQuillen. Bubble Point Measurements With Liquid Methane of a Screen Capillary Acquisition Device. NASA/TM-2009-215496. March 2009.
- [12] John M. Jurns., and John B. McQuillen. Liquid Acquisition Device Testing with Sub-Cooled Liquid Oxygen. AIAA 2008-4943. July 2008.
- [13] Michael Conrath., and Michael Dreyer Gas breakthrough at a porous screen. International Journal of Multiphase Flow (2012) 29-41.
- [14] K.-H. Grote., and J. Feldhusen. Dubbel – Taschenbuch für den Maschinenbau. 22ste Auflage. Springer-Verlag Berlin Heidelberg New York. 2007.
- [15] REFPROP. Reference Fluid Thermodynamic and Transport Properties. NIST Standard Reference Database 23. Version 8.0. Physical and Chemical Properties Division. 2007.
- [16] VDI-Wärmeatlas. Verein Deutscher Ingenieure. VDI-Gesellschaft Verfahrenstechnik und Chemieingenieurwesen (GVC). 10te Auflage. 2005.
- [17] H. Landolt., and H. Börnstein. Surface Tension of Pure Liquids and Binary Liquid Mixtures. Vol IV/24. Springer-Verlag Berlin Heidelberg. 2008.